

Hadron Properties with FLIC Fermions

J.M. Zanotti^{1,2}, D.B. Leinweber¹, W. Melnitchouk³, A.G. Williams¹, and
J.B. Zhang¹

¹ Department of Physics and Mathematical Physics and
Special Research Centre for the Subatomic Structure of Matter,
University of Adelaide, 5005, Australia

² John von Neumann-Institut für Computing NIC,
Deutsches Elektronen-Synchrotron DESY, D-15738 Zeuthen, Germany

³ Jefferson Lab, 12000 Jefferson Avenue, Newport News, VA 23606

Abstract. The Fat-Link Irrelevant Clover (FLIC) fermion action provides a new form of nonperturbative $\mathcal{O}(a)$ -improvement in lattice fermion actions offering near continuum results at finite lattice spacing. It provides computationally inexpensive access to the light quark mass regime of QCD where chiral nonanalytic behaviour associated with Goldstone bosons is revealed. The motivation and formulation of FLIC fermions, its excellent scaling properties and its low-lying hadron mass phenomenology are presented.

1 Introduction

The origin of the masses of light hadrons represents one of the most fundamental challenges to QCD. Despite the universal acceptance of QCD as the basis from which to derive hadronic properties, there has been slow progress in understanding the generation of hadron mass from first principles. Solving the problem of the hadronic mass spectrum would allow considerable improvement in our understanding of the nonperturbative nature of QCD. The only available method at present to derive hadron masses directly from QCD is a numerical calculation on the lattice.

The high computational cost required to perform accurate lattice calculations at small lattice spacings has led to increased interest in quark action improvement. In this article we present results of simulations of the spectrum of light mesons and baryons using an $\mathcal{O}(a)$ improved fermion action [1–4]. In particular, we will start with the standard clover action and replace the links in the irrelevant operators with APE smeared [5,6], or fat links. We shall refer to this action as the Fat-Link Irrelevant Clover (FLIC) action. Although the idea of using fat links only in the irrelevant operators of the fermion action was developed here independently, suggestions have appeared previously [7].

In Section 2, we provide the reader with some background information on lattice fermion actions. In particular, we start with the basic lattice discretisation of the derivative appearing in the continuum Dirac action, followed by improvements suggested first by Wilson [8] and then by Sheikholeslami and Wolhert [9]. Section 3 contains the procedure for creating the FLIC fermion action while

in Section 4 we describe the gauge configurations used in our lattice simulations. The results of an investigation of the scaling of this action at finite lattice spacing are presented in Section 5. In Section 6 we investigate the problem of exceptional configurations by performing simulations of hadron masses at light quark masses corresponding to $m_\pi/m_\rho = 0.35$. Section 7 discusses the evidence for enhancement in octet-decuplet mass splittings as one approaches the chiral limit in the quenched approximation and finally in Section 8 we summarise the results.

2 The Lattice Quark Action

2.1 The Naive Fermion Action

In Euclidean space-time, the continuum Dirac action is written as

$$\bar{\psi} (\not{D} + m) \psi, \quad (1)$$

where the covariant derivative is defined as $D_\mu = \partial_\mu + i g A_\mu$. Wilson [8] discretised the continuum Dirac action by replacing the derivative with a symmetrised finite difference. Gauge links are included to not only encode the gluon field, A_μ , but to also maintain gauge invariance

$$\bar{\psi} \not{D} \psi = \frac{1}{2a} \bar{\psi}(x) \sum_\mu \gamma_\mu \left[U_\mu(x) \psi(x + a\hat{\mu}) - U_\mu^\dagger(x - a\hat{\mu}) \psi(x - a\hat{\mu}) \right]. \quad (2)$$

Our notation uses the Pauli (Sakurai) representation of the Dirac γ -matrices defined in Appendix B of Sakurai [10]. In particular, the γ -matrices are hermitian, $\gamma_\mu = \gamma_\mu^\dagger$ and $\sigma_{\mu\nu} = [\gamma_\mu, \gamma_\nu]/(2i)$ such that $\gamma_\mu \gamma_\nu = \delta_{\mu\nu} + i \sigma_{\mu\nu}$. The gauge link variables at space-time position x are defined as

$$U_\mu(x) = \mathcal{P} \exp \left\{ i g \int_0^a A_\mu(x + \lambda\hat{\mu}) d\lambda \right\}. \quad (3)$$

Here the operator \mathcal{P} path-orders the A_μ 's along the integration path, a is the lattice spacing, and g is the coupling constant.

The continuum Dirac action is recovered in the limit $a \rightarrow 0$ by Taylor expanding the U_μ and $\psi(x+a\hat{\mu})$ in powers of the lattice spacing a . Keeping only the leading term in a (and for ease of notation we write $a\hat{\mu} \rightarrow \hat{\mu}$), Eq. (2) becomes

$$\begin{aligned} & \frac{1}{2a} \bar{\psi}(x) \gamma_\mu \left[\left(1 + i a g A_\mu(x + \frac{\hat{\mu}}{2}) + \dots \right) (\psi(x) + a \psi'(x) + \dots) - \right. \\ & \quad \left. \left(1 - i a g A_\mu(x - \frac{\hat{\mu}}{2}) + \dots \right) (\psi(x) - a \psi'(x) + \dots) \right] \\ & = \bar{\psi}(x) \gamma_\mu (\partial_\mu + \mathcal{O}(a^2)) \psi(x) + i g \bar{\psi}(x) \gamma_\mu [A_\mu + \mathcal{O}(a^2)] \psi(x), \end{aligned} \quad (4)$$

which is the kinetic part of the standard continuum Dirac action in Euclidean space-time to $\mathcal{O}(a^2)$. Hence we arrive at the simplest (“naive”) lattice fermion

action,

$$\begin{aligned}
 S_N &= m_q \sum_x \bar{\psi}(x) \psi(x) + \\
 &\quad \frac{1}{2a} \sum_{x,\mu} \bar{\psi}(x) \gamma_\mu \left[U_\mu(x) \psi(x + \hat{\mu}) - U_\mu^\dagger(x - \hat{\mu}) \psi(x - \hat{\mu}) \right] \\
 &\equiv \sum_x \bar{\psi}(x) M_{xy}^N[U] \psi(y),
 \end{aligned} \tag{5}$$

where the interaction matrix M^N is

$$M_{i,j}^N[U] = m_q \delta_{ij} + \frac{1}{2a} \sum_\mu [\gamma_\mu U_{i,\mu} \delta_{i,j-\mu} - \gamma_\mu U_{i-\mu,\mu}^\dagger \delta_{i,j+\mu}]. \tag{6}$$

The Taylor expansion in Eq. (4) shows that the naive fermion action of Eq. (5) has $\mathcal{O}(a^2)$ errors. It also preserves chiral symmetry. However, in the continuum limit it gives rise to $2^d = 16$ flavours of quark rather than one. This is the famous doubling problem and is easily demonstrated by considering the inverse of the free field propagator (obtained by taking the fourier transform of the action with all $U_\mu = 1$)

$$S^{-1}(p) = m_q + \frac{i}{a} \sum_\mu \gamma_\mu \sin p_\mu a, \tag{7}$$

which has 16 zeros within the Brillouin cell in the limit $m_q \rightarrow 0$. eg, $p_\mu = (0, 0, 0, 0)$, $(\pi/a, 0, 0, 0)$, $(\pi/a, \pi/a, 0, 0)$, etc. Consequently, this action is phenomenologically not acceptable.

There are two approaches commonly used to remove these doublers. The first involves adding operators to the quark action which scale with the lattice spacing and thus vanish in the continuum limit. These operators are chosen to drive the doublers to high energies and hence are suppressed. This technique for improving fermion actions proceeds via the improvement scheme proposed by Symanzik [11] and is discussed in more detail in the following sections. The second method for removing doublers involves ‘‘staggering’’ the quark degrees of freedom on the lattice. This procedure exploits the fact that the naive fermion action has a much larger symmetry group, $U_V(4) \otimes U_A(4)$, to reduce the doubling problem from $2^d = 16 \rightarrow 16/4$ while maintaining a remnant chiral symmetry. This approach is not used in this article so the details of the action will not be discussed here. Details of the derivation of staggered fermions can be found in most texts (eg. [12,13]).

2.2 Wilson Fermions

In order to avoid the doubling problem, Wilson [8] originally introduced an irrelevant (energy) dimension-five operator (the ‘‘Wilson term’’) to the standard naive lattice fermion action (Eq. (5)), which explicitly breaks chiral symmetry

at $\mathcal{O}(a)$.

$$S_W = \bar{\psi}(x) \left[\sum_{\mu} \left(\gamma_{\mu} \nabla_{\mu} - \frac{1}{2} r a \Delta_{\mu} \right) + m \right] \psi(x), \quad (8)$$

where r is the ‘‘Wilson coefficient,’’

$$\nabla_{\mu} \psi(x) = \frac{1}{2a} [U_{\mu}(x) \psi(x + \hat{\mu}) - U_{\mu}^{\dagger}(x - \hat{\mu}) \psi(x - \hat{\mu})], \quad (9)$$

and

$$\Delta_{\mu} \psi(x) = \frac{1}{a^2} [U_{\mu}(x) \psi(x + \hat{\mu}) + U_{\mu}^{\dagger}(x - \hat{\mu}) \psi(x - \hat{\mu}) - 2\psi(x)]. \quad (10)$$

The Wilson action in Eq. (8) has no doublers for $r > 0$ as the Wilson term gives the extra fifteen species at $p_{\mu} = \pi/a$ a mass proportional to r/a . Also, if $r = 1$ then the Wilson action has no ghost branches in its dispersion relation (see, for example, Ref. [14]). In terms of link variables, $U_{\mu}(x)$, the Wilson action can be written

$$S_W = \left(m_q + \frac{4r}{a} \right) \sum_x \bar{\psi}(x) \psi(x) + \frac{1}{2a} \sum_{x,\mu} \bar{\psi}(x) \left[(\gamma_{\mu} - r) U_{\mu}(x) \psi(x + \hat{\mu}) - (\gamma_{\mu} + r) U_{\mu}^{\dagger}(x - \hat{\mu}) \psi(x - \hat{\mu}) \right], \quad (11)$$

$$\equiv \sum_{x,y} \bar{\psi}_x^L M_{xy}^W \psi_y^L, \quad (12)$$

where the interaction matrix for the Wilson action, M^W , is usually written

$$M_{xy}^W[U] a = \delta_{xy} - \kappa \sum_{\mu} \left[(r - \gamma_{\mu}) U_{x,\mu} \delta_{x,y-\mu} + (r + \gamma_{\mu}) U_{x-\mu,\mu}^{\dagger} \delta_{x,y+\mu} \right], \quad (13)$$

with a field renormalisation

$$\begin{aligned} \kappa &= 1/(2m_q a + 8r), \\ \psi^L &= \psi/\sqrt{2\kappa}. \end{aligned} \quad (14)$$

We take the standard value $r = 1$ and the quark mass is given by

$$m_q a = \frac{1}{2} \left(\frac{1}{\kappa} - \frac{1}{\kappa_c} \right). \quad (15)$$

In the free theory the critical value of kappa, κ_c , where the quark mass vanishes, is $1/8r$. In the interacting theory, κ_c is renormalised away from $1/8r$. The quark mass has both multiplicative and additive renormalisations due to the explicit breaking of chiral symmetry by the Wilson term.

In the continuum limit, one finds

$$S_W = \int d^4x \bar{\psi}(x) \left(\not{D} + m - \frac{a r}{2} \sum_{\mu} D_{\mu}^2 \right) \psi(x) + \mathcal{O}(a). \quad (16)$$

By lifting the mass of the unwanted doublers with a second derivative, $\mathcal{O}(a)$ discretisation errors have been introduced into the fermion matrix. In contrast, the Wilson gauge action [8] has only $\mathcal{O}(a^2)$ errors. Hence there is enormous interest in applying Symanzik's improvement program [11] to the fermion action to remove $\mathcal{O}(a)$ errors by adding additional higher dimension terms.

2.3 Improving The Fermion Action

The addition of the Wilson term to the fermion action introduces large $\mathcal{O}(a)$ errors which means that in order to extrapolate reliably to the continuum limit, simulations must be performed on fine lattices, which are therefore very computationally expensive. The scaling properties of the Wilson action at finite a can be improved by introducing any number of irrelevant operators of increasing dimension whose contributions vanish in the continuum limit.

The first attempt at removing these $\mathcal{O}(a)$ errors was by Hamber and Wu [15] who added a two link term to the Wilson action

$$S_{HW} = S_W + \kappa \sum_{x,\mu} \left[\bar{\psi}^L(x) \left(-\frac{1}{4}r + \frac{1}{8}\gamma_\mu \right) U_\mu(x) U_\mu(x + \hat{\mu}) \psi^L(x + 2\hat{\mu}) \right. \\ \left. + \bar{\psi}^L(x + 2\hat{\mu}) \left(-\frac{1}{4}r - \frac{1}{8}\gamma_\mu \right) U_\mu^\dagger(x + \hat{\mu}) U_\mu^\dagger(x) \psi^L(x) \right]. \quad (17)$$

The removal of the classical $\mathcal{O}(a)$ terms is easily observed through a Taylor expansion. While this action also removes $\mathcal{O}(a^2)$ errors at tree-level, it has only received a small amount of interest due to the computational expense in evaluating the double hopping term. Calculations that have been done with this action show that it works well at coarse lattice spacings and has the added bonus that it has an improved dispersion relation [16].

A more systematic approach [11] to $\mathcal{O}(a)$ improvement of the lattice fermion action in general [9] is to consider all possible gauge invariant, local dimension-five operators, respecting the symmetries of QCD

$$\begin{aligned} \mathcal{O}_1 &= -\frac{ig a C_{SW} r}{4} \bar{\psi} \sigma_{\mu\nu} F_{\mu\nu} \psi, \\ \mathcal{O}_2 &= c_2 a \left\{ \bar{\psi} D_\mu D_\mu \psi + \bar{\psi} \overleftarrow{D}_\mu \overleftarrow{D}_\mu \psi \right\}, \\ \mathcal{O}_3 &= \frac{b_g a m_q}{2} \text{tr} \{ F_{\mu\nu} F_{\mu\nu} \}, \\ \mathcal{O}_4 &= c_4 m_q \left\{ \bar{\psi} \gamma_\mu D_\mu \psi - \bar{\psi} \overleftarrow{D}_\mu \gamma_\mu \psi \right\}, \\ \mathcal{O}_5 &= -b_m a m_q^2 \bar{\psi} \psi. \end{aligned} \quad (18)$$

Note that the operator $\mathcal{D}\mathcal{D}$ is linearly related to \mathcal{O}_1 and \mathcal{O}_2 as

$$\mathcal{D}\mathcal{D} = D_\mu D_\mu - \frac{g}{2} \sigma_{\mu\nu} F_{\mu\nu}. \quad (19)$$

Operator \mathcal{O}_1 is a new local operator in the lattice fermion action and must be included. On the other hand, \mathcal{O}_3 and \mathcal{O}_5 of Eq. (18) act to simply renormalise the coefficients of existing terms in the lattice action, removing $\mathcal{O}(a m_q)$ terms from the relation between bare and renormalised quantities. For example, the renormalisation of the quark mass $m_q \rightarrow m_q (1 - b_m a m_q)$ incorporates \mathcal{O}_5 . Similarly, \mathcal{O}_3 introduces a mass dependence in the gauge coupling $g^2 \rightarrow g^2 (1 - b_g a m_q)$ such that the lattice spacing remains constant for constant g as m_q is varied [17]. For the quenched approximation, $b_g = 0$.

The key observation to efficient $\mathcal{O}(a)$ improvement is that the $\mathcal{O}(a)$ improvement afforded by two-link terms of the fermion action [18] may be incorporated to $\mathcal{O}(a)$ into the standard Wilson fermion action complemented by \mathcal{O}_1 through the following transformation of the fermion fields

$$\begin{aligned}\psi &\rightarrow \psi' = (1 + b_q r a m_q) (1 - c_q r a \overleftrightarrow{D}) \psi, \\ \bar{\psi} &\rightarrow \bar{\psi}' = (1 + b_q r a m_q) \bar{\psi} (1 + c_q r a \overleftarrow{D}),\end{aligned}\quad (20)$$

where ψ' represents the physical fermion field recovered in the continuum limit, while ψ is the lattice fermion field used in the numerical simulations. The Jacobian of the transformation is 1 to $\mathcal{O}(a)$ [9]. At tree-level, $b_q = c_q = 1/4$ correctly incorporates the $\mathcal{O}(a)$ corrections of \mathcal{O}_2 and \mathcal{O}_4 into the fermion action. Note that this field transformation renormalises the fermion mass of the simulations

$$m \rightarrow m(1 + \frac{1}{2} r a m). \quad (21)$$

For the spectral quantities investigated herein, it is sufficient to work with the lattice fermion-field operators alone. Here the fermion operators, act only as interpolators between the QCD vacuum and the state of interest and do not affect the eigenstates of the QCD Hamiltonian. However, for matrix elements of fermion operators, hadron decay constants, or off-shell quantities such as the quark propagator, it is important to take this field redefinition into account to connect the lattice field operators to the continuum field operators incorporating important $\mathcal{O}(a)$ contributions.

In summary, \mathcal{O}_1 , the ‘‘clover’’ term, is the only dimension-five operator explicitly required to complement the Wilson action to obtain $\mathcal{O}(a)$ improvement. This particular action is known as the Sheikholeslami-Wohlert fermion [9] action

$$S_{SW} = S_W - \frac{i g a C_{SW} r}{4} \bar{\psi}(x) \sigma_{\mu\nu} F_{\mu\nu} \psi(x), \quad (22)$$

where C_{SW} is the clover coefficient which can be tuned to remove $\mathcal{O}(a)$ artifacts to all orders in the gauge coupling constant g .

$$C_{SW} = \begin{cases} 1 & \text{at tree-level,} \\ 1/u_0^3 & \text{mean-field improved,} \end{cases} \quad (23)$$

with u_0 the tadpole improvement factor correcting for the quantum renormalisation of the operators (see definition in Section 4). Nonperturbative (NP) $\mathcal{O}(a)$

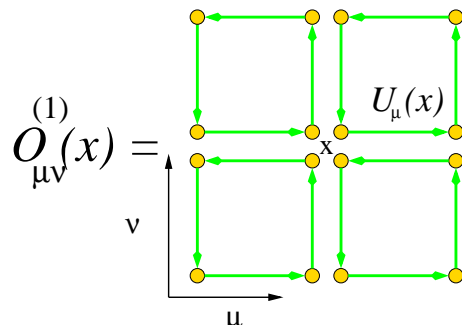


Fig. 1. Loops required to construct $F_{\mu\nu}$

improvement [19] uses the axial Ward identity to tune C_{SW} and remove all $\mathcal{O}(a)$ artifacts provided one simultaneously improves the coupling g^2 , the quark mass m_q , and the currents [19]. The advantage of the clover action is that it is local and is only a small overhead on Wilson fermion simulations. Further details of the improvement the clover action provides at finite lattice spacing is given in Section 5.

The name “clover” is associated with the SW fermion action due to the lattice discretisation of the field strength tensor, $F_{\mu\nu}$. An expression for $F_{\mu\nu}$ is obtained by considering the sum of the four 1×1 link paths surrounding any lattice site in the $\mu - \nu$ plane as shown in Fig. 1. Using the expansion for the elementary link product (see for example Ref. [12,13,20]), we obtain the lattice expression for $F_{\mu\nu}$

$$g a^2 F_{\mu\nu}(x) = \frac{1}{8i} \left[\left(\mathcal{O}_{\mu\nu}^{(1)}(x) - \mathcal{O}_{\mu\nu}^{(1)\dagger}(x) \right) - \frac{1}{3} \text{Tr} \left(\mathcal{O}_{\mu\nu}^{(1)}(x) - \mathcal{O}_{\mu\nu}^{(1)\dagger}(x) \right) \right], \quad (24)$$

where $F_{\mu\nu}$ is made traceless by subtracting 1/3 of the trace from each diagonal element and

$$\begin{aligned} \mathcal{O}_{\mu\nu}^{(1)}(x) &= U_\mu(x) U_\nu(x + \hat{\mu}) U_\mu^\dagger(x + \hat{\nu}) U_\nu^\dagger(x) \\ &+ U_\nu(x) U_\mu^\dagger(x + \hat{\nu} - \hat{\mu}) U_\nu^\dagger(x - \hat{\mu}) U_\mu(x - \hat{\mu}) \\ &+ U_\mu^\dagger(x - \hat{\mu}) U_\nu^\dagger(x - \hat{\mu} - \hat{\nu}) U_\mu(x - \hat{\mu} - \hat{\nu}) U_\nu(x - \hat{\nu}) \\ &+ U_\nu^\dagger(x - \hat{\nu}) U_\mu(x - \hat{\nu}) U_\nu(x + \hat{\mu} - \hat{\nu}) U_\mu^\dagger(x). \end{aligned} \quad (25)$$

Substantial progress has been made to improve $F_{\mu\nu}$ to $\mathcal{O}(a^6)$ by adding terms constructed using larger loops [20].

3 Fat-Link Irrelevant Fermion Action

The established approach to nonperturbative (NP) improvement [19] tunes the coefficient of the clover operator to all powers in g^2 . Unfortunately, this formulation of the clover action is susceptible to the problem of exceptional configurations as the quark mass becomes small. Chiral symmetry breaking in the clover fermion action introduces an additive mass renormalisation into the Dirac operator that can give rise to singularities in quark propagators at small quark masses. In practice, this prevents the simulation of small quark masses and the use of coarse lattices ($\beta < 5.7 \sim a > 0.18$ fm) [21,22]. Furthermore, the plaquette version of $F_{\mu\nu}$, which is commonly used in Eq. (22), has large $\mathcal{O}(a^2)$ errors, which can lead to errors of the order of 10% in the topological charge even on very smooth configurations [23].

The idea of using fat links in fermion actions was first explored by the MIT group [24] and more recently has been studied by DeGrand *et al.* [21,25,26], who showed that the exceptional configuration problem can be overcome by using a fat-link (FL) clover action. Moreover, the renormalisation of the coefficients of action improvement terms is small. In principle it is acceptable to smear the links of the relevant operators. The symmetry of the APE smearing process ensures that effects are $\mathcal{O}(a^2)$. The factors multiplying the link and staple ensure the leading order term is e^{iagA_μ} , an element of SU(3). Issues of projecting the smeared links to SU(3) are $\mathcal{O}(a^2)$ effects and therefore correspond to irrelevant operators [27]. However, the net effect of APE smearing the links of the relevant operators is to remove gluon interactions at the scale of the cutoff. While this has some tremendous benefits, the short-distance quark interactions are lost. As a result decay constants and vector-pseudoscalar mass splittings of heavy mesons, which are sensitive to the wave function at the origin, are suppressed [28].

The solution to this is to work with two sets of links in the fermion action. In the relevant dimension-four operators, one works with the untouched links generated via Monte Carlo methods, while the smeared fat links are introduced only in the higher dimension irrelevant operators. The effect this has on decay constants and vector-pseudoscalar mass splittings of heavy mesons is under investigation and will be reported elsewhere.

Fat links [21,25] are created by averaging or smearing links on the lattice with their nearest neighbours in a gauge covariant manner (APE smearing). The smearing procedure [5,6] replaces a link, $U_\mu(x)$, with a sum of the link and α times its staples

$$\begin{aligned}
 U_\mu(x) \rightarrow U'_\mu(x) = & (1 - \alpha) U_\mu(x) + \frac{\alpha}{6} \sum_{\substack{\nu=1 \\ \nu \neq \mu}}^4 \left[U_\nu(x) U_\mu(x + \hat{\nu}) U_\nu^\dagger(x + \hat{\mu}) \right. \\
 & \left. + U_\nu^\dagger(x - \hat{\nu}) U_\mu(x - \hat{\nu}) U_\nu(x - \hat{\nu} + \hat{\mu}) \right], \quad (26)
 \end{aligned}$$

followed by projection back to SU(3). We select the unitary matrix U_μ^{FL} which maximises

$$\text{Re tr}(U_\mu^{\text{FL}} U_\mu^\dagger),$$

by iterating over the three diagonal SU(2) subgroups of SU(3). Performing eight iterations over these subgroups gives gauge invariance up to seven significant figures. We repeat the combined procedure of smearing and projection n times. We create our fat links by setting $\alpha = 0.7$ and comparing $n = 4$ and 12 smearing sweeps. The mean-field improved FLIC action now becomes

$$S_{\text{SW}}^{\text{FL}} = S_{\text{W}}^{\text{FL}} - \frac{i g C_{\text{SW}} \kappa r}{2(u_0^{\text{FL}})^4} \bar{\psi}(x) \sigma_{\mu\nu} F_{\mu\nu} \psi(x), \quad (27)$$

where $F_{\mu\nu}$ is constructed using fat links, u_0^{FL} is calculated in an analogous way to Eq. (33) with fat links, and where the mean-field improved Fat-Link Irrelevant Wilson action is

$$S_{\text{W}}^{\text{FL}} = \sum_x \bar{\psi}(x) \psi(x) + \kappa \sum_{x,\mu} \bar{\psi}(x) \left[\gamma_\mu \left(\frac{U_\mu(x)}{u_0} \psi(x + \hat{\mu}) - \frac{U_\mu^\dagger(x - \hat{\mu})}{u_0} \psi(x - \hat{\mu}) \right) - r \left(\frac{U_\mu^{\text{FL}}(x)}{u_0^{\text{FL}}} \psi(x + \hat{\mu}) + \frac{U_\mu^{\text{FL}\dagger}(x - \hat{\mu})}{u_0^{\text{FL}}} \psi(x - \hat{\mu}) \right) \right]. \quad (28)$$

As reported in Table 1, the mean-field improvement parameter for the fat links is very close to 1. Hence, the mean-field improved coefficient for C_{SW} is accurate.¹ It is in this way that the extensive task of non-perturbatively calculating the renormalisations of the improvement coefficients discussed in Sec. 2.3 is avoided. APE smearing the links of dimension five operators suppresses the renormalisation, allowing the precise matching of improvement coefficients with only tree-level knowledge of their values.

In addition, one can now use highly improved definitions of $F_{\mu\nu}$ (involving terms up to u_0^{12}), which give impressive near-integer results for the topological charge [20]. In particular, we employ the 3-loop $\mathcal{O}(a^4)$ -improved definition of $F_{\mu\nu}$ in which the standard clover-sum of four 1×1 loops lying in the μ, ν plane is combined with 2×2 and 3×3 loop clovers. Bilson-Thompson *et al.* [20] find

$$g F_{\mu\nu} = \frac{-i}{8} \left[\left(\frac{3}{2} W_{\mu\nu}^{1 \times 1} - \frac{3}{20 u_0^4} W_{\mu\nu}^{2 \times 2} + \frac{1}{90 u_0^8} W_{\mu\nu}^{3 \times 3} \right) - \text{h.c.} \right]_{\text{Traceless}} \quad (29)$$

where $W^{n \times n}$ is the clover-sum of four $n \times n$ loops and $F_{\mu\nu}$ is made traceless by subtracting $1/3$ of the trace from each diagonal element of the 3×3 colour matrix. This definition reproduces the continuum limit with $\mathcal{O}(a^6)$ errors. On approximately self-dual configurations, this operator produces integer topological charge to better than 4 parts in 10^4 . We also consider a 5-loop improved $F_{\mu\nu}$ for the $20^3 \times 40$ lattice at $\beta = 4.53$. Since the results for the 5-loop operator agree with the 3-loop version to better than 4 parts in 10^4 [20], we are effectively using the same action as far the scaling analysis is concerned.

The use of thin links in Eq. (28) ensures that the relevant dimension-four operators see all the dynamics of the Monte-Carlo generated gauge fields. Upon

¹ Our experience with topological charge operators suggests that it is advantageous to include u_0 factors, even as they approach 1.

Table 1. The value of the mean link for different numbers of APE smearing sweeps, n , at $\alpha = 0.7$ on a $16^3 \times 32$ lattice at $\beta = 4.60$ which corresponds to a lattice spacing of 0.122(2) fm set by the string tension.

n	u_0^{FL}	$(u_0^{\text{FL}})^4$
0	0.88894473	0.62445197
4	0.99658530	0.98641100
12	0.99927343	0.99709689

expanding the thin links in terms of the gauge potential, $\mathcal{O}(a^2)$ contributions of energy-dimension six are revealed, which, ideally, should be removed via the fat-link irrelevant operator procedure. Fortunately, actions with many irrelevant operators (*e.g.* the D_{234} action) can now be handled with confidence as tree-level knowledge of the improvement coefficients is sufficient. However, as we will see, the scaling of the $\mathcal{O}(a)$ -improved FLIC fermion action of Eqs. (27) and (28) is excellent already, and the added computational expense of the two-link hopping terms required in $\mathcal{O}(a^2)$ -improvement is not well motivated at present.

Work by DeForcrand *et al.* [29] suggests that 7 cooling sweeps are required to approach topological charge within 1% of integer value. This is approximately 16 APE smearing sweeps at $\alpha = 0.7$ [30]. However, achieving integer topological charge is not necessary for the purposes of studying hadron masses, as has been well established. To reach integer topological charge, even with improved definitions of the topological charge operator, requires significant smoothing and associated loss of short-distance information. Instead, we regard this as an upper limit on the number of smearing sweeps.

Using unimproved gauge fields and an unimproved topological charge operator, Bonnet *et al.* [23] found that the topological charge settles down after about 10 sweeps of APE smearing at $\alpha = 0.7$. Consequently, we create fat links with APE smearing parameters $n = 12$ and $\alpha = 0.7$. This corresponds to ~ 2.5 times the smearing used in Refs. [21,25]. Further investigation reveals that improved gauge fields with a small lattice spacing ($a = 0.122$ fm) are smooth after only 4 sweeps. Hence, we perform calculations with 4 sweeps of smearing at $\alpha = 0.7$ and consider $n = 12$ as a second reference. Table 1 lists the values of u_0^{FL} for $n = 0, 4$ and 12 smearing sweeps.

We also compare our results with the standard Mean-Field Improved Clover (MFIC) action. We mean-field improve as defined in Eqs. (27) and (28) but with thin links throughout. For this action, the standard 1-loop definition of $F_{\mu\nu}$ is used.

4 Lattice Simulations

The simulations are performed using the Luscher-Weisz [31] mean-field improved, plaquette plus rectangle, gauge action on $12^3 \times 24$ and $16^3 \times 32$ lattices with

lattice spacings of 0.093, 0.122 and 0.165 fm determined from the string tension with $\sqrt{\sigma} = 440$ MeV. We define

$$S_G = \frac{5\beta}{3} \sum_{\text{sq}} \frac{1}{3} \mathcal{R}e \text{tr}(1 - U_{\text{sq}}(x)) - \frac{\beta}{12u_0^2} \sum_{\text{rect}} \frac{1}{3} \mathcal{R}e \text{tr}(1 - U_{\text{rect}}(x)), \quad (30)$$

where the operators $U_{\text{sq}}(x)$ and $U_{\text{rect}}(x)$ are defined as

$$U_{\text{sq}}(x) = U_\mu(x) U_\nu(x + \hat{\mu}) U_\mu^\dagger(x + \hat{\nu}) U_\nu^\dagger(x), \quad (31)$$

$$\begin{aligned} U_{\text{rect}}(x) &= U_\mu(x) U_\nu(x + \hat{\mu}) U_\nu(x + \hat{\nu} + \hat{\mu}) \\ &\quad \times U_\mu^\dagger(x + 2\hat{\nu}) U_\nu^\dagger(x + \hat{\nu}) U_\nu^\dagger(x) \\ &\quad + U_\mu(x) U_\mu(x + \hat{\mu}) U_\nu(x + 2\hat{\mu}) \\ &\quad \times U_\mu^\dagger(x + \hat{\mu} + \hat{\nu}) U_\mu^\dagger(x + \hat{\nu}) U_\nu^\dagger(x). \end{aligned} \quad (32)$$

The link product $U_{\text{rect}}(x)$ denotes the rectangular 1×2 and 2×1 plaquettes, and for the tadpole improvement factor we employ the plaquette measure

$$u_0 = \left(\frac{1}{3} \mathcal{R}e \text{tr} \langle U_{\text{sq}} \rangle \right)^{1/4}. \quad (33)$$

Initial studies of FLIC, mean-field improved clover and Wilson quark actions were made using 50 configurations. The scaling analysis of FLIC fermions was performed with a total of 200 configurations at each lattice spacing and volume. In addition, for the light quark simulations, 94 configurations are used on a $20^3 \times 40$ lattice with $a = 0.134(2)$ fm. Gauge configurations are generated using the Cabibbo-Marinari pseudo-heat-bath algorithm with three diagonal $SU(2)$ subgroups looped over twice. Simulations are performed using a parallel algorithm with appropriate link partitioning [32], and the error analysis is performed by a third-order, single-elimination jackknife, with the χ^2 per degree of freedom (N_{DF}) obtained via covariance matrix fits.

A fixed boundary condition is used for the fermions by setting

$$U_t(\mathbf{x}, nt) = 0 \quad \text{and} \quad U_t^{\text{FL}}(\mathbf{x}, nt) = 0 \quad \forall \mathbf{x} \quad (34)$$

in the hopping terms of the fermion action. The fermion source is centered at the space-time location $(x, y, z, t) = (1, 1, 1, 3)$, which allows for two steps backward in time without loss of signal, for all simulations except those on the $20^3 \times 40$ lattice at $\beta = 4.53$ which has the fermion source located at $(x, y, z, t) = (1, 1, 1, 8)$. Gauge-invariant Gaussian smearing [33] in the spatial dimensions is applied at the source to increase the overlap of the interpolating operators with the ground states. The source-smearing technique [33] starts with a point source,

$$\psi_0^a_\alpha(\mathbf{x}, t) = \delta^{ac} \delta_{\alpha\gamma} \delta_{\mathbf{x}, \mathbf{x}_0} \delta_{t, t_0} \quad (35)$$

for source colour c , Dirac γ , position $\mathbf{x}_0 = (1, 1, 1)$ and time t_0 and proceeds via the iterative scheme,

$$\psi_i(\mathbf{x}, t) = \sum_{\mathbf{x}'} F(\mathbf{x}, \mathbf{x}') \psi_{i-1}(\mathbf{x}', t),$$

where

$$F(\mathbf{x}, \mathbf{x}') = \frac{1}{(1 + \alpha)} \left(\delta_{\mathbf{x}, \mathbf{x}'} + \frac{\alpha}{6} \sum_{\mu=1}^3 \left[U_{\mu}(\mathbf{x}, t) \delta_{\mathbf{x}', \mathbf{x} + \hat{\mu}} + U_{\mu}^{\dagger}(\mathbf{x} - \hat{\mu}, t) \delta_{\mathbf{x}', \mathbf{x} - \hat{\mu}} \right] \right).$$

Repeating the procedure N times gives the resulting fermion source

$$\psi_N(\mathbf{x}, t) = \sum_{\mathbf{x}'} F^N(\mathbf{x}, \mathbf{x}') \psi_0(\mathbf{x}', t). \quad (36)$$

The parameters N and α govern the size and shape of the smearing function. We simulate with $N = 20$ and $\alpha = 6$, except on the $20^3 \times 40$ lattice which has $N = 35$. The propagator, S , is obtained from the smeared source by solving

$$M_{\alpha\beta}^{ab} S_{\beta\gamma}^{bc} = \psi_{\alpha}^a, \quad (37)$$

for each colour, Dirac source c , γ respectively of Eq. (35) via the BiStabilised Conjugate Gradient algorithm [34].

5 Scaling of FLIC Fermions

Hadron masses are extracted from the Euclidean time dependence of the calculated two-point correlation functions. For baryons the correlation functions are given by

$$G(t; \mathbf{p}, \Gamma) = \sum_x e^{-i\mathbf{p}\cdot\mathbf{x}} \Gamma^{\beta\alpha} \langle \Omega | T[\chi^{\alpha}(x) \bar{\chi}^{\beta}(0)] | \Omega \rangle, \quad (38)$$

where χ are standard baryon interpolating fields, Ω represents the QCD vacuum, Γ is a 4×4 matrix in Dirac space, and α, β are Dirac indices. At large Euclidean times one has

$$G(t; \mathbf{p}, \Gamma) \simeq \frac{Z^2}{2E_p} e^{-E_p t} \text{tr}[\Gamma(-i\gamma \cdot p + M)], \quad (39)$$

where Z represents the coupling strength of $\chi(0)$ to the baryon, and $E_p = (\mathbf{p}^2 + M^2)^{1/2}$ is the energy. Selecting $\mathbf{p} = 0$ and $\Gamma = (1 + \gamma_4)/4$, the effective baryon mass is then given by

$$M(t) = \log[G(t)] - \log[G(t + 1)]. \quad (40)$$

Meson masses are determined via analogous standard procedures. The critical value of κ , κ_{cr} , is determined by linearly extrapolating m_{π}^2 as a function of m_q to zero.

Figure 2 shows the nucleon effective mass plot for the FLIC action on a $16^3 \times 32$ lattice at $\beta = 4.60$ which corresponds to a lattice spacing of 0.122(2) fm set by the string tension. The fat links are created with 4 APE smearing sweeps at $\alpha = 0.7$ (“FLIC4”). The effective mass plots for the other hadrons are similar, and all display acceptable plateau behavior. Good values of χ^2/N_{DF} are obtained

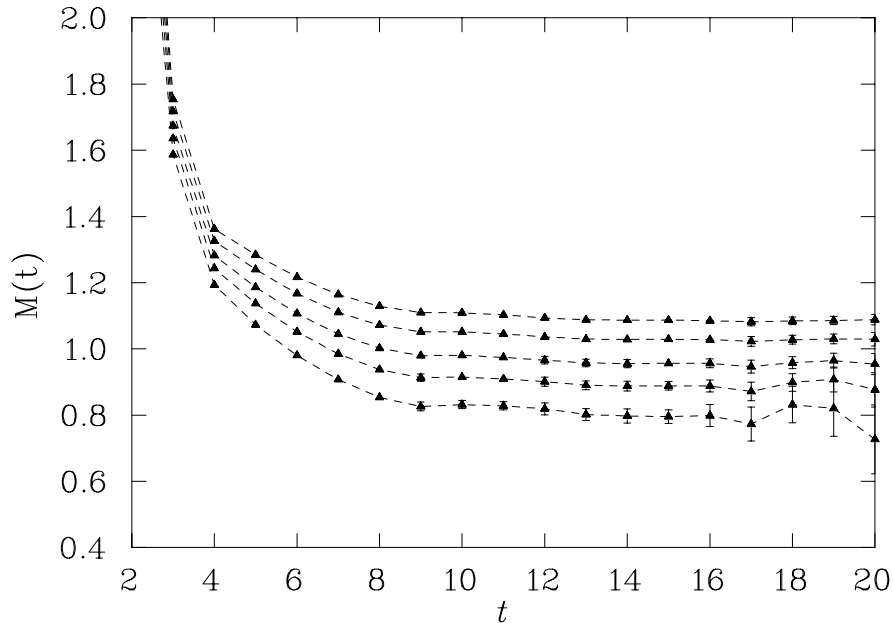


Fig. 2. Effective mass plot for the nucleon for the FLIC action from 200 configurations on a $16^3 \times 32$ lattice at $\beta = 4.60$ which corresponds to a lattice spacing of $0.122(2)$ fm set by the string tension. The fat links are created with 4 sweeps of smearing at $\alpha = 0.7$. The five sets of points correspond to the κ values listed in Table 2, with κ increasing from top down.

for many different time-fitting intervals as long as one fits after time slice 8. All fits for this action are therefore performed on time slices 9 through 14. For the Wilson action and the FLIC action with $n = 12$ (“FLIC12”), the effective mass plots look similar to Fig. 2 and display good plateau behavior. The fitting regimes used for these actions are 9-13 and 9-14, respectively.

The values of κ used in the simulations for all quark actions are given in Table 3. We have also provided the values of κ_{cr} for these fermion actions when using our mean-field improved, plaquette plus rectangle, gauge action at $\beta = 4.60$. We have mean-field improved our fermion actions so we expect the values for κ_{cr} to be close to the tree-level value of 0.125. Improved chiral properties are seen for the FLIC and MFIC actions, with FLIC4 performing better than FLIC12.

The behavior of the ρ , nucleon and Δ masses as a function of squared pion mass are shown in Fig. 3 for the various actions. The first feature to note is the excellent agreement between the FLIC4 and FLIC12 actions. On the other hand, the Wilson action appears to lie somewhat low in comparison. It is also reassuring that all actions give the correct mass ordering in the spectrum. The value of the squared pion mass at $m_\pi/m_\rho = 0.7$ is plotted on the abscissa for

Table 2. Values of κ and the corresponding π , ρ , N and Δ masses for the FLIC action with 4 sweeps of smearing at $\alpha = 0.7$ on a $16^3 \times 32$ lattice at $\beta = 4.60$. The value for κ_{cr} is provided in Table 3. A string tension analysis incorporating the lattice coulomb term provides $a = 0.122(2)$ fm for $\sqrt{\sigma} = 440$ MeV.

κ	$m_\pi a$	$m_\rho a$	$m_N a$	$m_\Delta a$
0.1260	0.5797(23)	0.7278(39)	1.0995(58)	1.1869(104)
0.1266	0.5331(24)	0.6951(45)	1.0419(64)	1.1387(121)
0.1273	0.4744(27)	0.6565(54)	0.9709(72)	1.0816(152)
0.1279	0.4185(30)	0.6229(65)	0.9055(82)	1.0310(194)
0.1286	0.3429(37)	0.5843(97)	0.8220(102)	0.9703(286)

Table 3. Values of κ and κ_{cr} for the four different actions on a $16^3 \times 32$ lattice at $\beta = 4.60$ which corresponds to a lattice spacing of 0.122(2) fm set by the string tension.

	Wilson	FLIC12	FLIC4	MFIC
κ_1	0.1346	0.1286	0.1260	0.1196
κ_2	0.1353	0.1292	0.1266	0.1201
κ_3	0.1360	0.1299	0.1273	0.1206
κ_4	0.1367	0.1305	0.1279	0.1211
κ_5	0.1374	0.1312	0.1286	0.1216
κ_{cr}	0.1390	0.1328	0.1300	0.1226

the three actions as a reference point. This point is chosen in order to allow comparison of different results by interpolating them to a common value of $m_\pi/m_\rho = 0.7$, rather than extrapolating them to smaller quark masses, which is subject to larger systematic and statistical uncertainties.

The scaling behaviour of the different actions is illustrated in Fig. 4. The present results for the Wilson action agree with those of Ref. [35]. The first feature to observe in Fig. 4 is that actions with fat-link irrelevant operators perform extremely well. For both the vector meson and the nucleon, the FLIC actions perform significantly better than the mean-field improved clover action. It is also clear that the FLIC4 action performs systematically better than the FLIC12. This suggests that 12 smearing sweeps removes too much short-distance information from the gauge-field configurations. On the other hand, 4 sweeps of smearing combined with our $\mathcal{O}(a^4)$ improved $F_{\mu\nu}$ provides excellent results, without the fine tuning of C_{SW} in the NP improvement program.

Notice that for the ρ meson, a linear extrapolation of previous mean-field improved clover results in Fig. 4 passes through our mean-field improved clover result at $a^2\sigma \sim 0.075$ which lies systematically low relative to the FLIC actions. However, a linear extrapolation does not pass through the continuum limit result, thus confirming the presence of significant $\mathcal{O}(a)$ errors in the mean-field improved clover fermion action. While there are no NP-improved clover plus improved

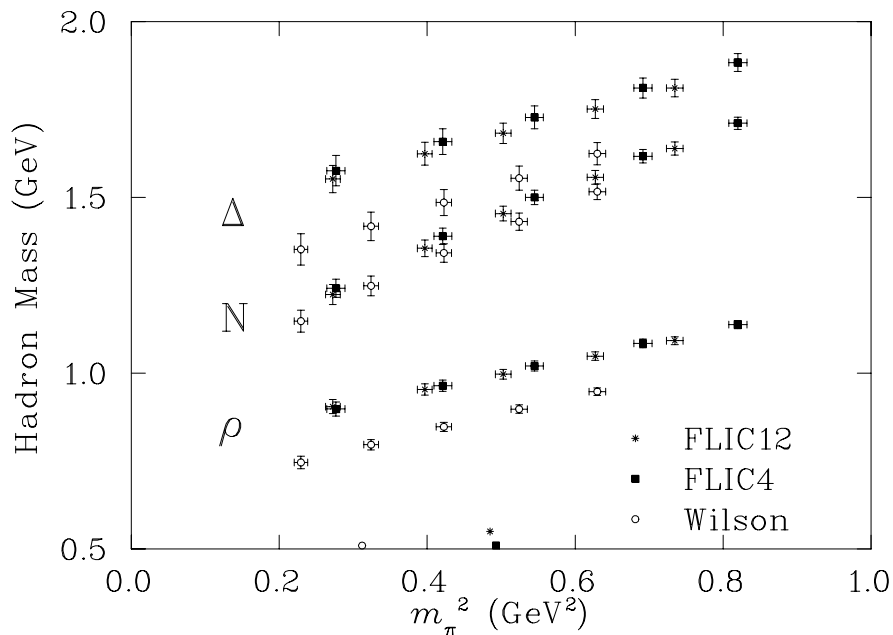


Fig. 3. Masses of the nucleon, Δ and ρ meson versus m_π^2 for the FLIC4, FLIC12 and Wilson actions on a $16^3 \times 32$ lattice at $\beta = 4.60$ which corresponds to a lattice spacing of 0.122(2) fm set by the string tension.

Table 4. String tensions, β , volumes and results for the vector meson and nucleon masses interpolated to $m_P/m_V = 0.7$. The scale for the small $\beta = 4.60$ lattice estimates are taken from the large $\beta = 4.60$ lattice

β	Volume	N_{configs}	$a\sqrt{\sigma}$	$m_v/\sqrt{\sigma}$	$m_N/\sqrt{\sigma}$	u_0
4.38	$16^3 \times 32$	200	0.371	2.378(25)	3.450(35)	0.8761
4.53	$20^3 \times 40$	94	0.299	2.318(18)	3.408(26)	0.8859
4.60	$12^3 \times 24$	200	0.274	2.434(26)	3.554(33)	0.8889
4.60	$16^3 \times 32$	200	0.274	2.336(22)	3.400(26)	0.8889
4.80	$16^3 \times 32$	200	0.210	2.427(23)	3.538(61)	0.8966

glue simulation results at $a^2\sigma \sim 0.075$, the simulation results that are available indicate that the fat-link results also compete well with those obtained with a NP-improved clover fermion action.

Having determined FLIC4 is the preferred action, we have increased the number of configurations to 200 for this action. As expected, the error bars are halved and the central values for the FLIC4 points move to the upper end of the error bars on the 50 configuration result, further supporting the promise of excellent scaling.

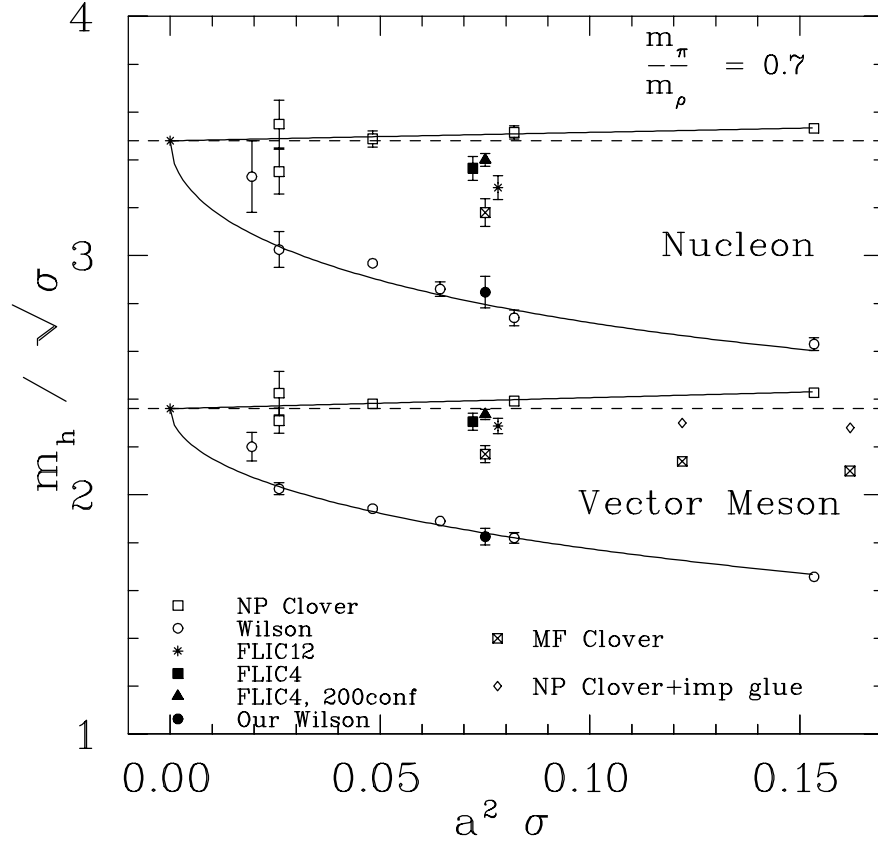


Fig. 4. Nucleon and vector meson masses for the Wilson, NP-improved, mean-field clover and FLIC actions. Results from the present simulations, based on 50 configurations and indicated by the solid points, are obtained by interpolating the results of Fig. 3 to $m_\pi/m_\rho = 0.7$. The fat links are constructed with $n = 4$ (solid squares) and $n = 12$ (stars) smearing sweeps at $\alpha = 0.7$. The solid triangles are results for the FLIC4 action when 200 configurations are used in the analysis. The FLIC results are offset from the central value for clarity. Our MF clover result at $a^2\sigma \sim 0.075$ lies systematically low relative to the FLIC actions.

In order to further test the scaling of the FLIC action at different lattice spacings, we consider four different lattice spacings and three different volumes. String tensions, volumes and hadron masses are given in Table 4 and the results are displayed in Fig. 5. The two different volumes used at $a^2\sigma \sim 0.075$ indicate a small finite volume effect, which increases the mass for the smaller volume at $a^2\sigma \sim 0.075$ and ~ 0.045 . Examination of points from the small and large volumes separately indicates continued scaling toward the continuum limit. While the finite volume effect will produce a different continuum limit value, the slope

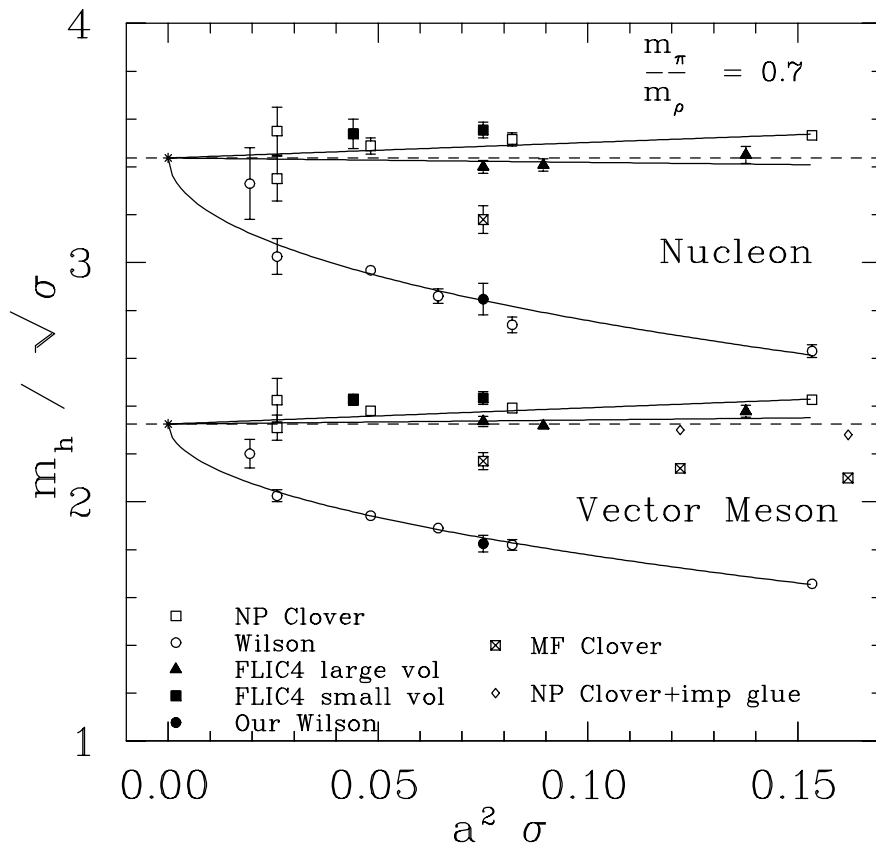


Fig. 5. Nucleon and vector meson masses for the Wilson, Mean-Field (MF) improved clover, NP-improved clover and FLIC actions obtained by interpolating simulation results to $m_\pi/m_\rho = 0.7$. For the FLIC action (“FLIC4”), fat links are constructed with $n = 4$ APE-smearing sweeps with smearing fraction $\alpha = 0.7$, except for the point at $a^2\sigma \sim 0.09$ which has $n = 6$. Results from the current simulations are indicated by the solid symbols; those from earlier simulations by open or hatched symbols. The solid-lines illustrate fits, constrained to have a common continuum limit, to FLIC, NP-improved clover and Wilson fermion action results obtained on physically large lattice volumes.

of the points from the smaller and larger volumes agree, consistent with errors of $\mathcal{O}(a^2)$.

Focusing on simulation results from physical volumes with extents ~ 2 fm and larger, we perform a simultaneous fit of the FLIC, NP-improved clover and Wilson fermion action results. The fits are constrained to have a common continuum limit and assume errors are $\mathcal{O}(a^2)$ for FLIC and NP-improved clover actions and $\mathcal{O}(a)$ for the Wilson action. An acceptable χ^2 per degree of freedom

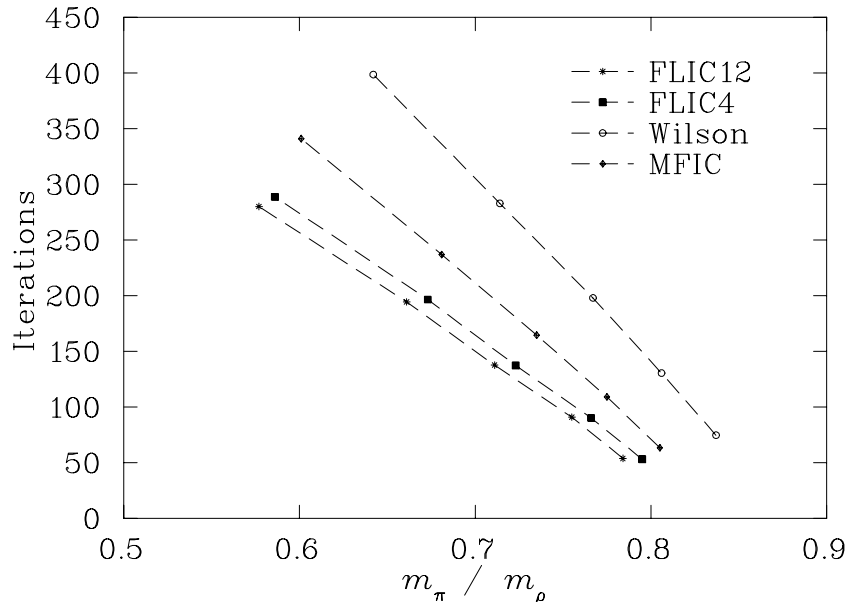


Fig. 6. Average number of stabilised biconjugate gradient iterations for the Wilson, FLIC and mean-field improved clover (MFIC) actions plotted against m_π/m_ρ . The fat links are constructed with $n = 4$ (solid squares) and $n = 12$ (stars) smearing sweeps at $\alpha = 0.7$ on a $16^3 \times 32$ lattice at $\beta = 4.60$ which corresponds to a lattice spacing of $0.122(2)$ fm set by the string tension.

is obtained for both the nucleon and ρ -meson fits. These results indicate that FLIC fermions provide a new form of nonperturbative $\mathcal{O}(a)$ improvement. The FLIC fermion results display nearly perfect scaling indicating $\mathcal{O}(a^2)$ errors are small for this action.

6 Search For Exceptional Configurations

Chiral symmetry breaking in the Wilson action allows continuum zero modes of the Dirac operator to be shifted into the negative mass region. This problem is accentuated as the gauge fields become rough ($a \rightarrow$ large). Local lattice artifacts at the scale of the cutoff (often referred to as dislocations) give rise to spurious near zero modes. The quark propagator can then encounter singular behaviour as the quark mass becomes light.

Exceptional configurations are a severe problem in quenched QCD (QQCD) because instantons are low action field configurations which appear readily in QQCD. These instanton configurations give rise to approximate zero modes which should be suppressed at light quark masses by $\det M$ which is present

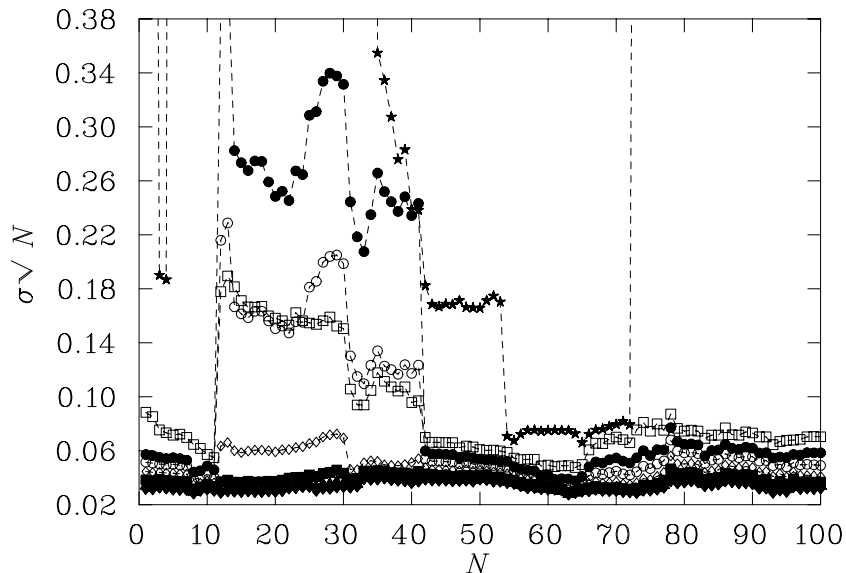


Fig. 7. The standard deviation in the error of the π mass for eight quark masses (with the star symbols being the lightest quark mass) calculated on 30 configurations plotted against the starting configuration number for the FLIC-fermion action on a $20^3 \times 40$ lattice with $a = 0.134(2)$ fm.

in the link updates in full QCD. This determinant is not present in QQCD and as a result, near-zero modes are overestimated in the ensemble.

The addition of the clover term to the fermion action broadens the distribution of near-zero modes. As a result, the clover action is notorious for revealing the exceptional configuration problem in QQCD. The FLIC action is expected to reduce the number of exceptional configurations by smoothing the gauge fields of the irrelevant operator via APE smearing [5,6]. The smoothing procedure has the effect of suppressing the local lattice artifacts and narrowing the distribution of near-zero modes, enabling simulations to be performed at light quark masses not currently accessible with the standard mean-field or non-perturbative improved clover fermion actions.

In order to access the light quark regime, we would like our preferred action to be efficient when inverting the fermion matrix. Fig. 6 compares the convergence rates of the different actions on a $16^3 \times 32$ lattice at $\beta = 4.60$ by plotting the number of stabilised biconjugate gradient [34] iterations required to invert the fermion matrix as a function of m_π/m_ρ . For any particular value of m_π/m_ρ , the FLIC actions converge faster than both the Wilson and mean-field improved clover fermion actions. Also, the slopes of the FLIC lines are smaller in magnitude than those for Wilson and mean-field improved clover actions, which provides great promise for performing cost effective simulations at quark masses closer

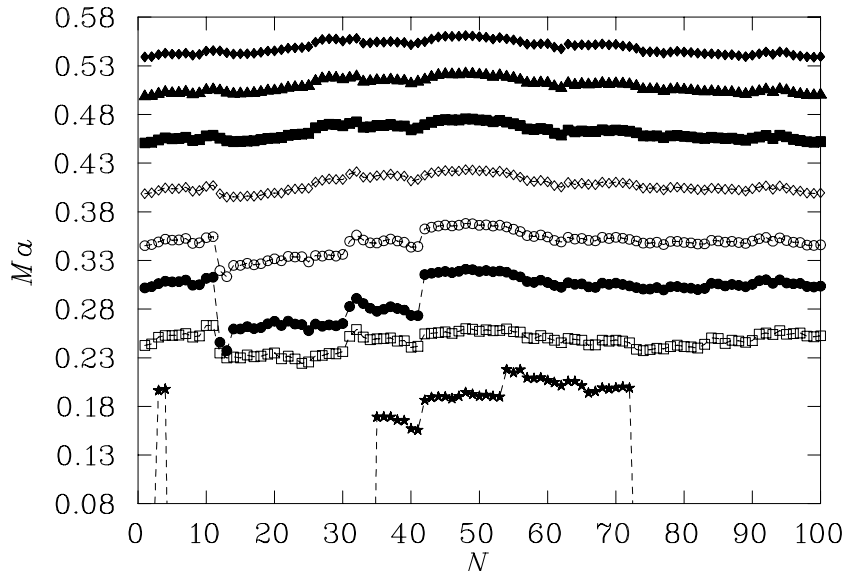


Fig. 8. The π mass calculated for eight quark masses (with the star symbols being the lightest quark mass) on 30 configurations plotted against the starting configuration number for the FLIC-fermion action on a $20^3 \times 40$ lattice with $a = 0.134$ fm.

to the physical values. Problems with exceptional configurations have prevented such simulations in the past.

The ease with which one can invert the fermion matrix using FLIC fermions (also see Ref [36]) leads us to attempt simulations down to light quark masses corresponding to $m_\pi/m_\rho = 0.35$. Previous attempts with Wilson-style fermion actions on configurations with lattice spacing ≥ 0.1 fm have only succeeded in getting down to $m_\pi/m_\rho = 0.47$ [37]. In order to search for exceptional configurations, we follow the technique used by Della Morte *et al.* [37] and note that in the absence of exceptional configurations, the standard deviation of an observable will be independent of the number of configurations considered in the average. Exceptional configurations reveal themselves by introducing a significant jump in the standard deviation as the configuration is introduced into the average. In severe cases, exceptional configurations can lead to divergences in correlation functions or prevent the matrix inversion process from converging.

The simulations are on a $20^3 \times 40$ lattice with a lattice spacing of 0.134(2) fm set by a string tension analysis incorporating the lattice coulomb term. The physical length of the lattice is ~ 2.7 fm. We have used an initial set of 100 configurations, using $n = 6$ sweeps of APE-smearing and a five-loop improved lattice field-strength tensor. Fig. 7 shows the standard deviation of the pion mass for eight quark masses on subsets of 30 (consecutive) configurations with a cyclic property enforced from configuration 100 to configuration 1. At first

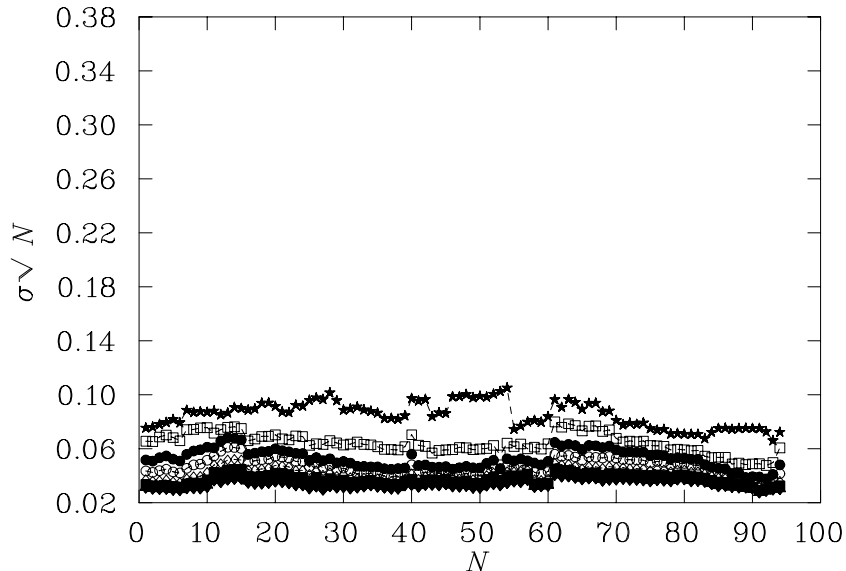


Fig. 9. The standard deviation in the error of the π mass for eight quark masses (with the star symbols being the lightest quark mass) calculated on 30 configurations plotted against the starting configuration number for the FLIC-fermion action on a $20^3 \times 40$ lattice with $a = 0.134$ fm. Configuration numbers 2, 13, 30, 34, 41 and 53 have been omitted.

glance, it is obvious that the error blows up for several quark masses at $N = 12$ and drops again at $N = 42$. As configurations 12 through 41 are included in the average at $N = 12$, this indicates that configuration number 41 is a candidate for an exceptional configuration. An inspection of the pion mass in Fig. 8 shows that the pion mass for the third lightest quark mass decreases significantly more than the second or fourth lightest quark masses. This indicates that κ_{cr} for this configuration lies somewhere between κ_6 and κ_7 . A solution to this problem would be to use the modified quenched approximation (MQM) from Ref. [22] and move κ_{cr} on this configuration back to the ensemble average for κ_{cr} . However, since the movement of κ_{cr} is largely a quenched artifact and would be suppressed in a full QCD simulation we prefer to simply identify and remove such configurations from the ensemble. Obviously, if we find that a significant percentage of our configurations are having trouble at a particular quark mass, then it would make no sense to proceed with the simulation. We would then have to conclude that we have reached the light quark mass limit of our action and simply step back to the next lightest mass.

Now let us return to Fig. 7. In addition to the highly exceptional configuration number 41, we also notice a large increase in error in the lightest quark mass for configuration numbers 2, 13, 30, 34 and 53. Upon removal of these con-

Table 5. Values of κ and the corresponding π , ρ , N and Δ masses on a $20^3 \times 40$ lattice for the FLIC action with 6 sweeps of smearing at $\alpha = 0.7$. A string tension analysis incorporating the lattice coulomb term provides $a = 0.134(2)$ fm for $\sqrt{\sigma} = 440$ MeV.

κ	$m_\pi a$	$m_\rho a$	$m_N a$	$m_\Delta a$
0.1278	0.5400(30)	0.7304(55)	1.0971(80)	1.2238(98)
0.1283	0.4998(31)	0.7053(58)	1.0522(84)	1.1899(102)
0.12885	0.4521(34)	0.6774(63)	1.0006(91)	1.1528(108)
0.1294	0.3990(38)	0.6491(72)	0.9465(101)	1.1162(115)
0.1299	0.3434(43)	0.6228(87)	0.8944(116)	1.0841(125)
0.13025	0.2978(47)	0.6040(107)	0.8562(134)	1.0630(135)
0.1306	0.2419(54)	0.5845(143)	0.8172(171)	1.0443(154)
0.1308	0.1972(69)	0.5812(213)	0.7950(215)	1.0380(189)

figurations, we see in Fig. 9 a near-constant behaviour of the standard deviation for the remaining configurations. This means that our elimination rate for our FLIC6 action on a lattice with a spacing 0.134 fm is about 6%. So for the 100 configurations used in this analysis, we are able to use 94 of them to extract hadron masses.

A similar analysis on a $16^3 \times 32$ lattice at $\beta = 4.60$ providing a finer lattice spacing of 0.122(2) fm reveals a much smaller exceptional configuration rate. In a sample of 200 configurations, 4 were identified as exceptional. The increase from 2% to 6% in going from $a \simeq 0.125$ to 0.135 fm suggests that the coarser lattice spacing is near the limit of applicability for FLIC fermions in the light quark mass regime.

7 Octet-Decuplet Mass Splittings

The results presented in this section are based on an initial sample of 94 gauge-field configurations of an anticipated 400 configurations. Figure 10 shows the N and Δ masses as a function of m_π^2 for the FLIC-fermion action on $20^3 \times 40$ lattices with $a = 0.132$ fm (which corresponds to a string tension scale with $\sqrt{\sigma} = 450$ MeV) such that the nucleon extrapolation passes through the physical value for clarity. An upward curvature in the Δ mass for decreasing quark mass is observed in the FLIC fermion results. This behaviour, increasing the quenched $N - \Delta$ mass splitting, was predicted by Young *et al.* [38,39] using quenched chiral perturbation theory (Q χ PT) formulated with a finite-range regulator. A fit to the FLIC-fermion results is illustrated by the solid curves. The dashed curves estimate the correction that will arise in unquenching the lattice QCD simulations [38,39]. We note that after we have corrected for the absence of sea quark loops, our results agree simultaneously with the physical values for both the nucleon and Δ .

We also calculate the light quark mass behaviour of the octet and decuplet hyperons. The strange quark mass is chosen in order to reproduce the physical

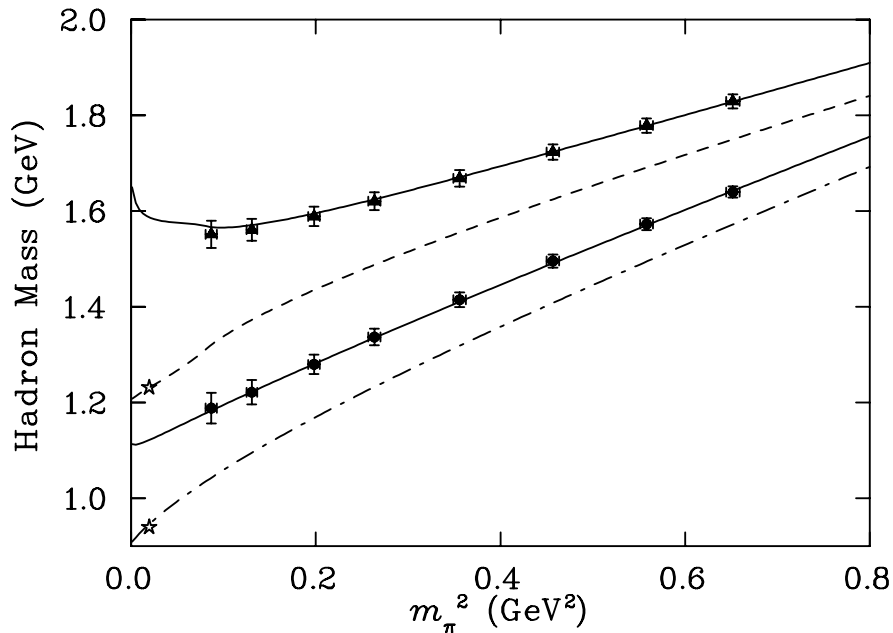


Fig. 10. Nucleon and Δ masses for the FLIC-fermion action on a $20^3 \times 40$ lattice. Here we select $a = 0.132$ fm (which corresponds to the string tension with $\sqrt{\sigma} = 450$ MeV) such that the nucleon extrapolation passes through the physical value for clarity. The solid curves illustrate fits of finite-range regularised quenched chiral perturbation theory [38,39] to the lattice QCD results. The dashed curves estimate the correction that will arise in unquenching the lattice QCD simulations [38,39]. Stars at the physical pion mass denote experimentally measured values.

strange quark mass according to the phenomenological value of an $s\bar{s}$ pseudoscalar meson,

$$m_{s\bar{s}}^2 = 2m_K^2 - m_\pi^2. \quad (41)$$

Upon substitution of the physical masses for the π and K mesons, this corresponds to an $s\bar{s}$ pseudoscalar meson mass of ~ 0.470 GeV² which occurs at our third heaviest quark mass in the $20^3 \times 40$ lattice analysis. The results from this calculation are given in Table 6 and are illustrated in Fig. 11. The results show the correct ordering and in particular, we notice a mass splitting between the *strangeness* = -1 ($I = 1$) Σ and ($I = 0$) Λ baryons becoming evident in the light quark mass regime.

Just as we saw the non-analytic behaviour of quenched chiral perturbation theory in the Δ -baryon mass in Fig. 10 leading to an enhancement of the quenched $N - \Delta$ mass spitting, Fig. 12 shows a similar enhancement for the decuplet-octet mass splittings in Σ and Ξ baryons respectively. The quark

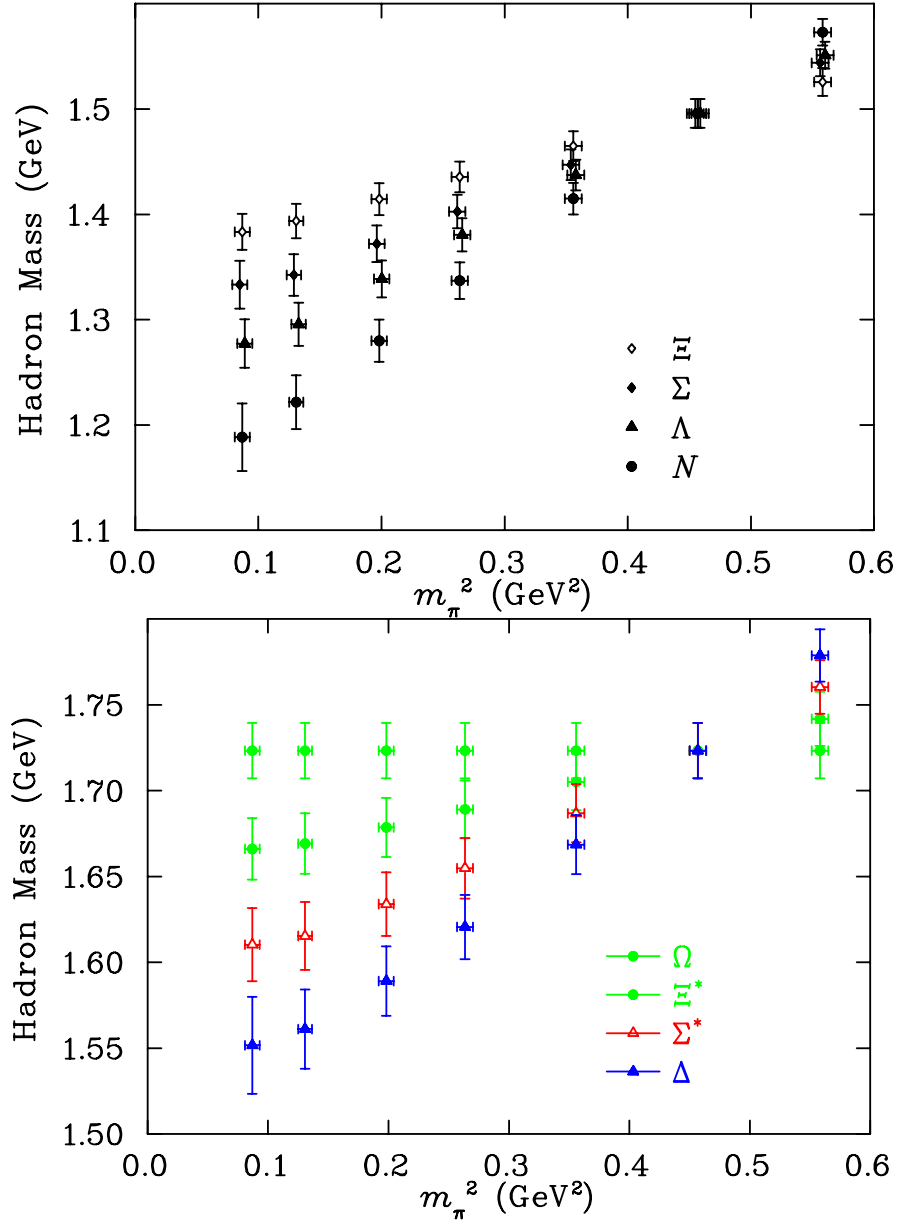


Fig. 11. Octet (top) and decuplet (bottom) baryon masses for the FLIC-fermion action on a $20^3 \times 40$ lattice with $a = 0.134$ fm.

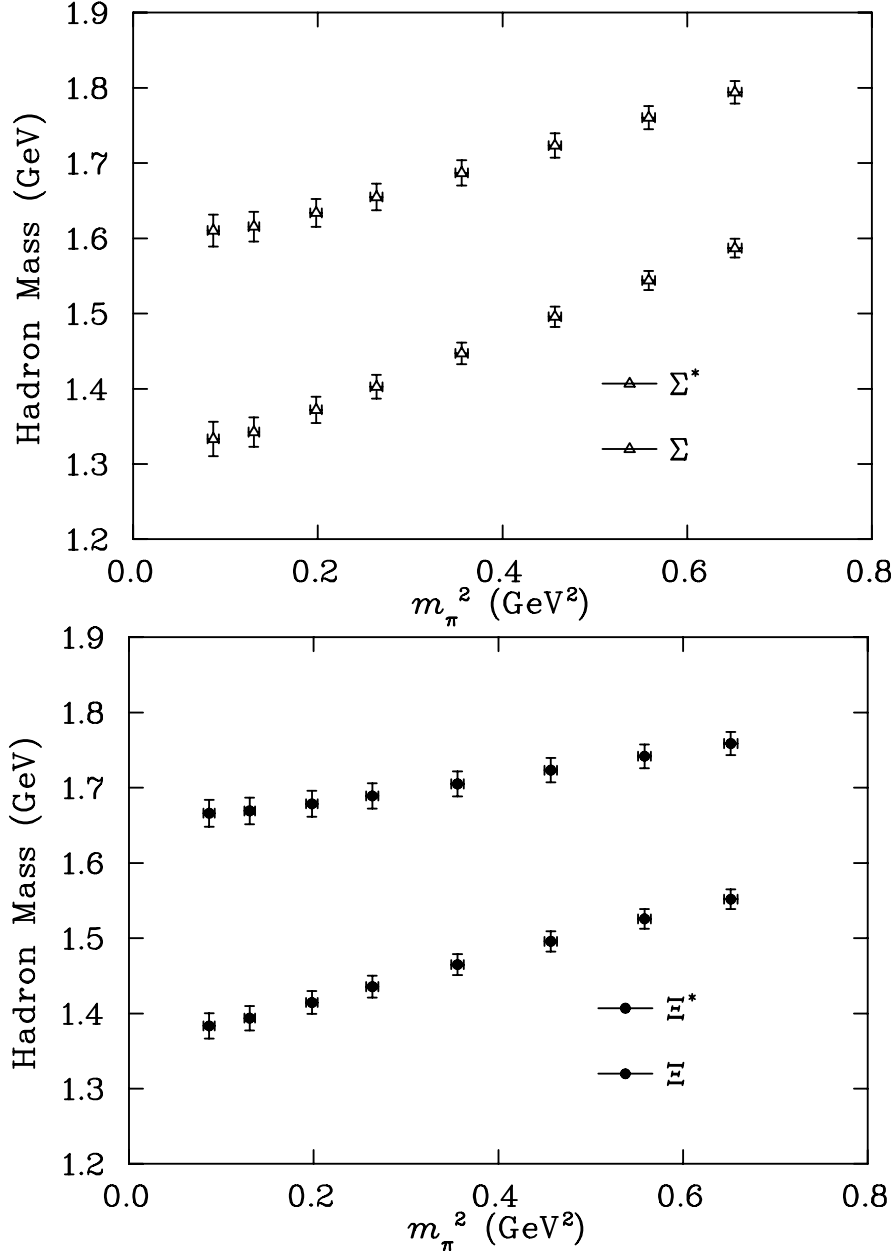


Fig. 12. Octet and decuplet baryon masses for Σ (top) and Ξ (bottom) for the FLIC-fermion action on a $20^3 \times 40$ lattice with $a = 0.134$ fm.

Table 6. Values of κ , the octet Λ , Σ , Ξ and decuplet Σ^* , Ξ^* masses on a $20^3 \times 40$ lattice for the FLIC action with 6 sweeps of smearing at $\alpha = 0.7$. A string tension analysis provides $a = 0.134(2)$ fm for $\sqrt{\sigma} = 440$ MeV.

κ	$m_\Lambda a$	$m_\Sigma a$	$m_\Xi a$	$m_{\Sigma^*} a$	$m_{\Xi^*} a$
0.1278	1.0696(84)	1.0616(83)	1.0381(87)	1.2002(101)	1.1765(104)
0.1283	1.0376(86)	1.0328(86)	1.0206(88)	1.1776(104)	1.1652(106)
0.12885	1.0006(91)	1.0006(91)	1.0006(91)	1.1528(108)	1.1528(108)
0.1294	0.9615(97)	0.9680(97)	0.9799(94)	1.1284(113)	1.1406(110)
0.1299	0.9235(106)	0.9383(106)	0.9603(98)	1.1070(118)	1.1299(113)
0.13025	0.8955(117)	0.9178(116)	0.9462(102)	1.0930(124)	1.1229(115)
0.1306	0.8667(137)	0.8980(132)	0.9323(109)	1.0806(132)	1.1166(118)
0.1308	0.8544(154)	0.8919(152)	0.9254(114)	1.0772(142)	1.1145(120)

model predicts that the hyperfine splittings should approximately satisfy [40]

$$\Xi_s^* - \Xi_s = \mu_s \mu_q = \Sigma_s^* - \Sigma_s, \quad (42)$$

where the baryon label denotes the hyperon mass and μ_s (μ_q) denotes the magnetic moment of the strange (light) constituent quark. Fig. 13 shows that even though the quenched approximation enhances the splitting between octet and decuplet baryons, the splittings for the Σ and Ξ baryons still satisfy Eq. (42). Agreement of the quenched QCD results with the quark model prediction is not surprising since both have a suppressed meson cloud. Similarly, one expects further suppression of the meson cloud when two (heavy) strange quarks are present in a baryon.

8 Summary

We have calculated hadron masses to test the scaling of the Fat-Link Irrelevant Clover (FLIC) fermion action, in which only the irrelevant, higher-dimension operators involve smeared links. One of the main conclusions of this work is that the use of fat links in the irrelevant operators provides a new form of nonperturbative $\mathcal{O}(a)$ improvement. This technique competes well with $\mathcal{O}(a)$ nonperturbative improvement on mean field-improved gluon configurations, with the advantage of a reduced exceptional configuration problem.

Quenched simulations at quark masses down to $m_\pi/m_\rho = 0.35$ have been successfully performed on a $20^3 \times 40$ lattice with a lattice spacing of $0.134(2)$ fm on 94 out of 100 configurations. Simulations at such light quark masses reveal the non-analytic behaviour of quenched chiral perturbation theory and provide for an interesting analysis of the hyperfine splittings between octet and decuplet baryons.

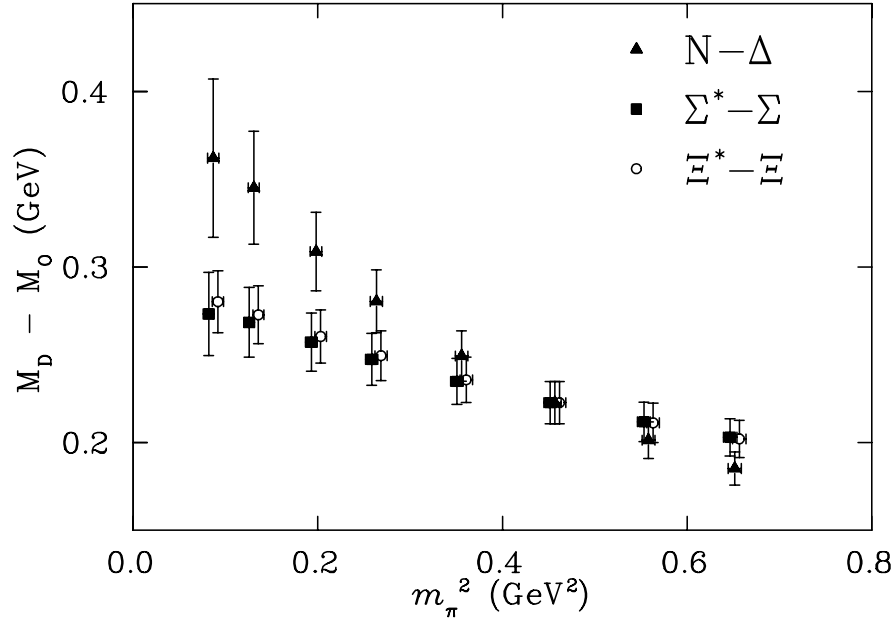


Fig. 13. Decuplet (M_D) - octet (M_O) baryon mass splittings for the FLIC-fermion action on a $20^3 \times 40$ lattice with $a = 0.132$ fm.

Acknowledgements

We thank Ross Young for contributing the fits of finite-range regularized quenched chiral perturbation theory to the FLIC fermion results illustrated in Fig. 10. Generous grants of supercomputer time from the Australian Partnership for Advanced Computing (APAC) and the Australian National Computing Facility for Lattice Gauge Theory are gratefully acknowledged. This work was supported in part by the Australian Research Council and by DOE contract DE-AC05-84ER40150 under which the Southeastern Universities Research Association (SURA) operates the Thomas Jefferson National Accelerator Facility.

References

1. J. M. Zanotti *et al.* [CSSM Lattice Collaboration], Phys. Rev. D **65**, 074507 (2002) hep-lat/0110216.
2. J. M. Zanotti *et al.*, Nucl. Phys. Proc. Suppl. **109**, 101 (2002) hep-lat/0201004.
3. J. M. Zanotti, D. B. Leinweber, W. Melnitchouk, A. G. Williams and J. B. Zhang, hep-lat/0210041.
4. D. B. Leinweber *et al.*, nucl-th/0211014.
5. M. Falcioni, M. L. Paciello, G. Parisi and B. Taglienti, Nucl. Phys. B **251**, 624 (1985).

6. M. Albanese *et al.* [APE Collaboration], Phys. Lett. B **192**, 163 (1987).
7. H. Neuberger, Phys. Rev. D **61**, 085015 (2000) hep-lat/9911004.
8. K. G. Wilson, CLNS-321 *New Phenomena In Subnuclear Physics. Part A. Proceedings of the First Half of the 1975 International School of Subnuclear Physics, Erice, Sicily, July 11 - August 1, 1975*, ed. A. Zichichi, Plenum Press, New York, 1977, p. 69, CLNS-321
9. B. Sheikholeslami and R. Wohlert, Nucl. Phys. B **259**, 572 (1985).
10. J. J. Sakurai, "Advanced Quantum Mechanics", Addison-Wesley, Redwood City, CA, 1982.
11. K. Symanzik, Nucl. Phys. B **226**, 187 (1983).
12. H. J. Rothe, World Sci. Lect. Notes Phys. **59**, 1 (1997).
13. R. Gupta, hep-lat/9807028.
14. M. G. Alford, T. R. Klassen and G. P. Lepage, Nucl. Phys. B **496**, 377 (1997) [arXiv:hep-lat/9611010].
15. H. W. Hamber and C. M. Wu, Phys. Lett. B **133**, 351 (1983).
16. F. X. Lee and D. B. Leinweber, Phys. Rev. D **59**, 074504 (1999) [hep-lat/9711044].
17. C. Dawson, G. Martinelli, G. C. Rossi, C. T. Sachrajda, S. R. Sharpe, M. Talevi and M. Testa, Nucl. Phys. Proc. Suppl. **63** (1998) 877 [hep-lat/9710027].
18. G. Heatlie, G. Martinelli, C. Pittori, G. C. Rossi and C. T. Sachrajda, Nucl. Phys. B **352** (1991) 266.
19. M. Luscher, S. Sint, R. Sommer and P. Weisz, Nucl. Phys. B **478**, 365 (1996), hep-lat/9605038.
20. S. O. Bilson-Thompson, D. B. Leinweber and A. G. Williams, Annals Phys. **304**, 1 (2003) [hep-lat/0203008].
21. T. DeGrand [MILC collaboration], Phys. Rev. D **60**, 094501 (1999) hep-lat/9903006.
22. W. Bardeen, A. Duncan, E. Eichten, G. Hockney and H. Thacker, Phys. Rev. D **57**, 1633 (1998) hep-lat/9705008.
23. F. D. Bonnet, P. Fitzhenry, D. B. Leinweber, M. R. Stanford and A. G. Williams, Phys. Rev. D **62**, 094509 (2000) hep-lat/0001018.
24. M. C. Chu, J. M. Grandy, S. Huang and J. W. Negele, Phys. Rev. D **49**, 6039 (1994) hep-lat/9312071.
25. T. DeGrand, A. Hasenfratz and T. G. Kovacs [MILC Collaboration], hep-lat/9807002.
26. M. Stephenson, C. DeTar, T. DeGrand and A. Hasenfratz, Phys. Rev. D **63**, 034501 (2001) hep-lat/9910023.
27. C. W. Bernard and T. DeGrand, Nucl. Phys. Proc. Suppl. **83**, 845 (2000) hep-lat/9909083.
28. C. Bernard *et al.* [MILC Collaboration], Phys. Rev. D **66**, 094501 (2002) hep-lat/0206016.
29. P. de Forcrand, M. Garcia Perez and I. O. Stamatescu, Nucl. Phys. B **499**, 409 (1997) hep-lat/9701012.
30. F. D. Bonnet, D. B. Leinweber, A. G. Williams and J. M. Zanotti, Phys. Rev. D **65**, 114510 (2002) hep-lat/0106023.
31. M. Luscher and P. Weisz, Commun. Math. Phys. **97**, 59 (1985) [Erratum-ibid. **98**, 433 (1985)].
32. F. D. Bonnet, D. B. Leinweber and A. G. Williams, J. Comput. Phys. **170**, 1 (2001) hep-lat/0001017.
33. S. Gusken, Nucl. Phys. Proc. Suppl. **17**, 361 (1990).
34. A. Frommer, V. Hannemann, B. Nockel, T. Lippert and K. Schilling, Int. J. Mod. Phys. C **5**, 1073 (1994) hep-lat/9404013.

35. R. G. Edwards, U. M. Heller and T. R. Klassen, Phys. Rev. Lett. **80**, 3448 (1998) hep-lat/9711052.
36. W. Kamleh, D. H. Adams, D. B. Leinweber and A. G. Williams, Phys. Rev. D **66**, 014501 (2002) hep-lat/0112041.
37. M. Della Morte, R. Frezzotti and J. Heitger [ALPHA collaboration], hep-lat/0111048.
38. R. D. Young, D. B. Leinweber, A. W. Thomas and S. V. Wright, Phys. Rev. D **66**, 094507 (2002) hep-lat/0205017.
39. R. D. Young, D. B. Leinweber and A. W. Thomas, arXiv:hep-lat/0311038.
40. F. E. Close, "An Introduction To Quarks And Partons", Academic Press, London, 1979, 481p.